

Structural investigation of the Be–W intermetallic system

A. Wiltner, F. Kost, S. Lindig, Ch. Linsmeier*

Max-Planck-Institut für Plasmaphysik, EURATOM Association,

Boltzmannstrasse 2, D-85748 Garching b. München, Germany

Abstract

The intermetallic Be–W system is investigated by analyzing both, a W film on polycrystalline Be and, the inverse system, Be films on polycrystalline W. The films are annealed up to 1070 K and the alloy formation is investigated by a combination of Rutherford backscattering spectroscopy (RBS) and X-ray photoelectron spectroscopy (XPS). For the structure analysis and identification of the formed alloys X-ray diffraction measurements (XRD) are used. In the case of W films on Be we identify Be_{12}W within the diffusion depth, whereas Be films

*Corresponding author, Tel.: +49-89-3299 2285, Fax.: +49-89-3299 962285,
e-mail: linsmeier@ipp.mpg.de

on W show alloy formation restricted to the film–substrate interface.

Both, XPS and XRD measurements indicate the formation of Be_2W .

1 Introduction

For the international tokamak experiment ITER, carbon (C), tungsten (W) and beryllium (Be) are planned to be the first wall materials. Therefore, the interactions between these components are of fundamental importance. The Be–W intermetallic system shows three different alloys, namely Be_2W , Be_{12}W and Be_{22}W [1]. Having different physical properties, it is important to know under which conditions the different alloys are formed. Since W is used in the divertor region due to the high melting point ($T_m = 3695$ K), the lower melting point of all known alloys is detrimental to the stability of these parts. Especially Be_{22}W ($T_m < 1800$ K) and Be_{12}W ($T_m < 2000$ K) have significantly lower melting points. Little is known on the reactivity of Be and W in the literature. Most data reported by now are measured as bulk data. We are interested in surface and near-surface processes, since two cases can be distinguished concerning processes in a fusion device. Namely, tungsten can be deposited onto a beryllium surface or vice versa. Thus, two approaches have been chosen in our investigations. A tungsten film has been prepared on a beryllium substrate as well as an inverse system. By this means, we can investigate diffusion or desorption processes and alloy formation. After preparation, the samples are heated up by progressive steps and investigated with Rutherford backscattering spectroscopy (RBS), X-ray

photoelectron spectroscopy (XPS) and X-ray diffraction (XRD). Whereas RBS and XPS measurements provide information on elemental composition and chemical states, the XRD powder patterns allow the identification of crystallographic phases.

2 Experimental

RBS is performed at the Garching 3 MV tandem accelerator (RBS with ^1H , ^3He and ^4He , scattering angle 165°). XPS analysis is performed in a PHI ESCA 5600 spectrometer. For these measurements, we use a monochromatic Al $K\alpha$ source ($h\nu = 1486.6$ eV) and an analyzed area of 0.8 mm in diameter. The sputter depth profiles are measured in this UHV chamber under an ion impact angle of 45° . For experimental details concerning both techniques and their combination we refer to [2].

The diffraction patterns are obtained by $\Theta/2\Theta$ scans using an X-ray diffractometer XRD 3003 PTS from Seifert equipped with a Cu anode. The samples are illuminated by an X-ray beam of about 3 mm diameter with the energy of the Cu $K\alpha_{1/2}$ lines ($\lambda = 1.541$ Å). For the Be film on W, we use a fixed incident angle of 1° with respect to the surface. This geometry is used for a low Z (Be) material with a low cross section for X-rays on a high Z (W) material leading to a higher surface sensitivity.

Two different systems are investigated in the experiments. For the first case, W on Be, a polycrystalline Be substrate ($1 \times 1 \text{ cm}^2$) is used. The W film (thickness 200 nm) is deposited in a magnetron sputter device (base pressure $2 \times 10^{-5} \text{ Pa}$). The Be substrate is etched in a pure Ar plasma before the layer deposition is started. The sample is then analyzed by RBS and XPS after applying thermal treatments. For the second case, Be on W, we use a polycrystalline W substrate ($1 \times 1 \text{ cm}^2$). These measurements are performed in a UHV chamber where surface analysis (using XPS) and sample preparation (cleaning and layer deposition) are possible without transfer through air. The W sample is cleaned using alternating sputter (3 keV Ar^+) and heating cycles (970 K) until no impurities are detected in the XPS spectra. The Be layers are deposited from a commercial evaporator (Omicron EFM3) using a BeO crucible filled with Be pieces (HEK GmbH, 99.999%). The base pressure in the UHV chamber is better than $2 \times 10^{-8} \text{ Pa}$. During the deposition procedure, the pressure is below $4 \times 10^{-8} \text{ Pa}$.

From the RBS spectra measured for the first system (W on Be), we get information about sample composition and depth distribution, whereas XPS analysis provides further information about sample composition in the near-surface region (several nanometers). Moreover, the chemical state of Be and W are determined from chemical shifts. After the final annealing step (1070 K, several hours), the sample is analyzed with a sputter depth profile

(3 keV Ar⁺) in the XPS chamber. From XRD measurements, we get information about both the structures of the layer and the substrate after the final annealing step. For the second system (Be on W), thermal treatment and XPS analysis are performed in the same UHV chamber without any transport through air. RBS measurements are not applied. Immediately after layer deposition, the sample is analyzed using XPS spectra in survey and high resolution modus. From the survey scans, the sample composition is estimated. From spectra obtained in the high resolution mode, information on the chemical states is gained from the shifts in the Be 1s and W 4f signals. The samples are annealed in steps of 100 K up to 1070 K and analyzed at room temperature. For the XRD analysis, we deposit Be on W (\gtrsim 50 nm) in a separate preparation sequence and anneal the sample up to 970 K for 90 min in UHV before the XRD measurements are performed.

3 Results and Discussion

3.1 W film on Be substrate

The results of RBS and XPS measurements are presented in detail at the PSI-17 conference in 2006 [2]. Here, we present a short summary. After each annealing step (up to 1070 K), the sample is analyzed with RBS. Spectra

obtained with ^1H and ^4He give information about changes in the W layer. Below 1000 K, the W layer is only barely affected. At 1070 K a beginning Be–W intermixing at the layer-substrate interface is observed. While the annealing time increases, the W intensity decreases, but the W is not completely lost into the Be bulk. The Be edge is also unaffected up to 970 K. After the first annealing step at 1070 K, an intermixing of W and Be is concluded from the position of the Be edge and an additional Be surface peak. W in the surface layer is replaced by Be. After the final annealing step at 1070 K, the Be surface signal vanishes and the RBS spectrum indicates a smooth Be depth distribution. From the ^1H and ^4He RBS measurements, the depth profiles are calculated. As it is observed in the RBS measurements, the Be–W intermixing begins above 1000 K and leads to a stable phase after 600 min at 1070 K. The stoichiometric ratio indicates the formation of Be_{12}W . The sample is then analyzed by a sputter depth profile in combination with XPS. After the removal of surface contaminations (C and O), we observe a constant sample composition (75.7% Be, 22.9% W and O) representing the Be–W intermetallic phase. XPS measurements in combination with sputter depth profiling do not represent the true stoichiometry of a compound due to preferential sputtering effects. In the high resolution spectra we observe an alloy component (111.3 eV) besides the metallic state (111.8 eV) within the Be 1s signal. The binding energy shift between these

components reaches -0.5 eV. At the outermost surface, intensity from BeO (114.8 eV) dominates the Be 1s signal. After removal of this BeO surface layer, the whole Be–W layer shows a constant composition within the Be 1s signal (65-70% alloy, 30% metal and < 5% BeO).

For the structural analysis of the Be–W layer, XRD measurements are performed. The diffraction diagram after the final annealing step at 1070 K is shown in the upper panel of Fig. 1. The reference data for Be and Be₁₂W in the lower panels are taken from the JCPDS-ICDD database [3]. The same reference patterns are estimated from the software package Diamond [4], taking into account the crystal structure of Be and Be₁₂W [5]. The structure parameter are as follows. Be is a metal with a hexagonal lattice structure (P6₃/mmc, a=2.286 Å, c=3.584 Å) and Be₁₂W shows a tetragonal unit cell (I4/mmm, a=7.220 Å, c=4.220 Å). From a comparison of measured and reference data, we conclude the formation of Be₁₂W. The respective references of Be₁₂W in the measured diffraction pattern are marked by ●. Additional peaks are from the Be substrate (■). In particular, no diffraction patterns originating from W, BeO and Be₂W are measured. Since we observe only Be and Be₁₂W signals, we conclude the formation of this alloy within the Be–W intermixing depth range. The Be pattern originates from the substrate. The diffusion of W and Be leads to the formation of an ordered alloy (Be₁₂W) in the Be–W layer, as it is also determined by RBS analysis and measured by

XPS sputter depth profile.

From the combination of RBS, XPS and XRD measurements, we conclude a Be–W intermixing above 1000 K with a formation of a constant alloy phase after long-term annealing at 1070 K. This alloy is identified as Be_{12}W .

3.2 Be films on W substrate

We already presented XPS measurements in [2, 6, 7] and give here a short summary. After room temperature deposition of Be layers from submonolayer coverage up to 4 nm thickness, we observe a Be–W surface alloy restricted to the interface. The surface alloy is visible in both signals ($< 10\%$ in Be $1s$ and W $4f$). Be deposited in excess is in the metallic state. We observe also BeO ($< 10\%$ in average) in the layer. Up to 670 K, the Be layer thickness and composition, respectively, remain constant. Above 670 K the Be layer thickness decreases and we observe an increase in the alloy intensities within the Be $1s$ (alloy at 111.1 eV, $\Delta\text{BE} = -0.7$ eV) and W $4f$ (alloy at 31.0 eV, $\Delta\text{BE} = -0.4$ eV) signals. The stoichiometric ratio of this alloy compound is $\text{Be}_{\leq 2}\text{W}$. The observation of a binding energy shift of -0.7 eV as compared to -0.5 eV, as given above for Be_{12}W , indicates the formation of a different alloy stoichiometry. From this observation and the stoichiometric ratio, we conclude the formation of Be_2W . The decrease of layer thickness

depends on the initially deposited amount. Thin Be layers (up to 1.2 nm) show no Be loss. If the initial coverage ranges from 1.2–~3.0 nm, the residual layer thicknesses are 1.4 nm in maximum. Thicker Be layers (> 3.0 nm) show a decelerated decrease with a residual thickness above 1.6 nm. In all cases an alloy phase (Be_2W) is observed at 970 K. Sputter depth profiles performed after the final annealing step indicate an intermixing of Be and W in restricted depth. Be diffusion into the W bulk is not observed. The Be loss during the thermal treatments is due to Be desorption rather than diffusion into greater depths.

For the XRD analysis, a thick Be film ($\gtrsim 50$ nm) is deposited on a W substrate in UHV. The layer thickness after room temperature deposition exceeds the information depth of XPS analysis (several nanometers) and a thickness estimation using Be and W signal intensities is not possible. The Be amount decreases while annealing at 970 K for 90 min, but a layer thickness estimation using XPS intensities from Be $1s$ and W $4f$ signals is still not possible. The high resolution XPS measurements of the Be $1s$ and W $4f$ signals immediately after the thermal treatment are dominated by intensities from the metallic states. Since XPS measurements are surface sensitive, we cannot analyze the Be–W intermixing layer at the film–substrate interface. These observations for the $\gtrsim 50$ nm Be film on W are compatible with and confirm the experiments described earlier [2, 6, 7]. During the thermal treatment at

970 K, we observe a decelerated Be loss compared to Be films of a few nm thickness. The detection of metallic states in both signals confirm the restriction of the Be–W intermixing to the interface at 970 K, as it is observed after deposition of thin Be films on W. In particular, no alloy formation throughout a larger Be thickness is observed, as it was shown for the first case (W on Be, see 3.1). We gain more information concerning the Be–W layer and interface composition from XRD measurements. The XRD pattern of the sample is shown in the upper panel of Fig. 2. The measured diffraction pattern is compared with XRD patterns (lower panels in Fig. 2) taken from the JCPDS database and calculated by the software package Diamond. The respective crystal structure data are taken from the ICSD database. W has a cubic crystal structure (Im-3m, $a=3.1652 \text{ \AA}$), BeO obtains a tetragonal unit cell (P4₂/mm, $a=4.750 \text{ \AA}$, $c=2.470 \text{ \AA}$) and Be₂W shows a hexagonal lattice structure (P6₃/mmc, $a=4.437 \text{ \AA}$, $c=7.347 \text{ \AA}$). The measured XRD pattern is dominated by the substrate (W). Additional reflexes with minor intensities, however, cannot be explained by W. These reflexes originate from Be. The reflexes originating from Be and W are identified by measuring reference samples and a comparison with reference data, respectively. The residual reflexes observed in the measured pattern cannot be clearly identified as BeO or Be₂W by comparing their positions with powder patterns originating from the JCPDS database and the software package Diamond, respectively. These

reference data are shown in the lower panels of Fig. 2. Diffraction patterns originating from Be_{12}W are not observed. Since Be is deposited onto W, the XRD measurements are performed by using a fixed incident angle of 1° with respect to the surface. However, XRD analysis is applied for the structural investigation of bulk materials and is not sensitive to small amounts of components or thin films. From the observation of W and Be, we conclude again a restriction of an intermixing of Be and W limited to the film–substrate interface, as it was already shown for the XPS measurements and sputter depth profiles of thin Be films on W. The alloy formation is observed in the XPS analysis, but the restriction to the interface doesn't allow an observation of the respective diffraction patterns in the XRD measurements.

After the XRD analysis, we perform a sputter depth profile in combination with XPS in high resolution mode. From this measurement, we gain information on the Be layer and, moreover, on the film–substrate interface composition. The near–surface region is dominated by contaminations (C and O) due to transport through air for the XRD analysis. After removal of this contaminated layer, we observe Be (90%) and O (10%) within the Be film. The Be $1s$ signal is dominated by intensities originating from metallic (70-80%) and oxidic Be (10% in average). The remaining signal intensity is at the position of the alloy component ($\Delta\text{BE} = -0.65$ eV). The measured composition of the Be layer and Be $1s$ signal, respectively, are comparable

to the values which are observed immediately after film deposition. After reaching the film–substrate interface, the intensity of the alloy component increases (60%). Metallic (30-40%) and oxidic Be (remaining intensity) are still observed. After removal of the Be–W intermixed layer the Be 1s signal vanishes. Intensity originating from the W 4*f* signal is detected when reaching the film–substrate interface. In the W 4*f*_{7/2} signal, we observe metallic W (~15%) and an alloy component (~40%, $\Delta BE = -0.4$ eV). As it was mentioned for the sputter depth profile for the W film on Be, we cannot determine the true stoichiometry of the alloy component with these measurements due to preferential sputtering effects. From the observation of an alloy component restricted to the film–substrate interface, we conclude again a limited diffusion of Be and W at 970 K. The observation of the chemical shifts within the Be 1s (-0.65 eV) and W 4*f* (-0.40 eV) signals and the stoichiometry of Be_{<2}W indicates the formation of the ordered alloy Be₂W. Metallic Be is detected in the layer, as it is also measured in the XRD analysis.

From XPS measurements of thin Be films on W and a XRD analysis combined with a XPS sputter depth profile of a thick Be film, we conclude the formation of Be₂W restricted to the film–substrate interface.

Thin Be films on W and the separately deposited Be film for XRD analysis are annealed up to 970 K. As it is shown in [6, 7], a thermal treatment up to 1070 K does not change the alloy amount within the Be 1s and W 4*f*

signal significantly. Long term annealing experiments for Be films on W at temperatures above 1000 K are not applied by now. The W films on Be are annealed up to 1070 K. Below this temperature no diffusion is observed. The W tiles in ITER are expected to operate at values below these temperatures. In addition, a Be deposition on W is more likely compared to W on Be. From a comparison of both experimental approaches, we conclude a limited diffusion of Be and W under ITER conditions and the formation of Be_2W rather than Be_{12}W or Be_{22}W .

4 Summary

The crystallographic structure of the Be–W intermetallic system is analyzed in detail in combination with additional qualitative and quantitative techniques. We deposit W films on Be and vice versa in order to determine diffusion and alloy formation of both metals. A W film on Be shows a Be–W intermixing above 1000 K and the final alloy is identified as Be_{12}W . This conclusion is drawn from the identification of the Be_{12}W diffraction pattern in XRD measurements, the constant stoichiometry in the RBS measurements and a binding energy shift within the Be 1s signal in the XPS analysis.

Since Be deposition on W is more likely under ITER conditions, also Be layers on polycrystalline W are investigated. Independent from the initially

deposited Be amount, the samples show a Be–W intermixing in restricted depth after annealing at 970 K. Be amounts in greater depth are not observed in sputter depth profiles after long-term annealing experiments up to 970 K. From the XRD analysis of a Be film after thermal treatment at 970 K and XPS binding energy shifts within the Be 1s and W 4*f* signals, the formation of Be₂W rather than Be₁₂W or Be₂₂W is concluded. The combination of XRD and XPS analysis affirm the observation of a restriction of Be–W intermixing.

Acknowledgements

We thank F. Koch for the preparation of W films on Be. The cooperation of K. Ertl and J. Roth in the analysis of the RBS data of the W/Be system is greatly appreciated.

References

- [1] T.B. Massalski, H. Okamoto, P.R. Subramanian, L. Kacprzak, Binary Alloy Phase Diagrams, 2nd ed. (1996).
- [2] Ch. Linsmeier, K. Ertl, J. Roth, A. Wiltner, K. Schmid, F. Kost, S. R. Bhattacharyya, M. Baldwin, R. P. Doerner, J. Nucl. Mat. (in press).

- [3] The international centre for diffraction data (ICDD), PDF database (2000), <http://www.icdd.com>.
- [4] Diamond, Version 3.1d, Crystal Impact GbR (2006).
- [5] Inorganic Crystal Structure Database, Version 1.3.3, NIST, FIZ Karlsruhe, Germany (2004).
- [6] A. Wiltner, Ch. Linsmeier, J. Nucl. Mat. 337-339 (2005) 951.
- [7] A. Wiltner, Ch. Linsmeier, New J. Phys. 8 (2006) 181.

Fig. 1

XRD analysis of a 200 nm thick W film on polycrystalline Be after the final annealing step at 1070 K. Reference data are given in the lower panels. Reflexes from Be substrate (■) and Be_{12}W (●) are marked.

Fig. 2

Analysis of a $\gtrsim 50$ nm thick Be film on polycrystalline W after annealing at 970 K and the identification of W (■) and Be (●). Reference data for Be_2W , Be, W and BeO are given in the panels below. The broad signal at 30° is an artifact due to the sample holder.

Figure 1:

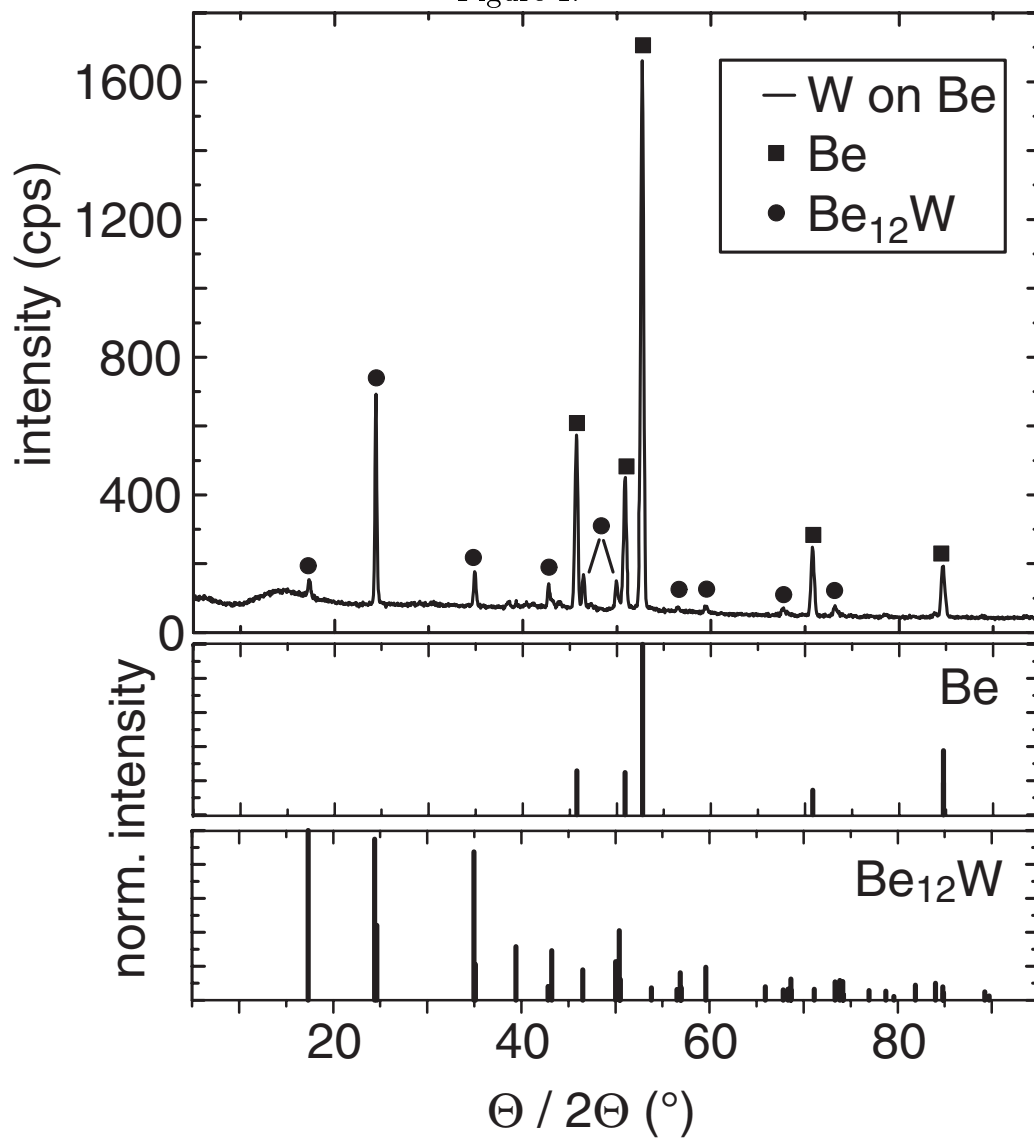


Figure 2:

